

---

# BOUNDMATCH: BOUNDARY DETECTION APPLIED TO SEMI-SUPERVISED SEGMENTATION FOR URBAN-DRIVING SCENES

---

A PREPRINT

**Haruya Ishikawa** **Yoshimitsu Aoki**  
Department of Electrical Engineering  
Keio University  
Yokohama, Japan  
haruyaishikawa@keio.jp

March 29, 2025

## ABSTRACT

Semi-supervised semantic segmentation (SS-SS) aims to mitigate the heavy annotation burden of dense pixel labeling by leveraging abundant unlabeled images alongside a small labeled set. While current teacher-student consistency regularization methods achieve strong results, they often overlook a critical challenge: the precise delineation of object boundaries. In this paper, we propose BoundMatch, a novel multi-task SS-SS framework that explicitly integrates semantic boundary detection into the consistency regularization pipeline. Our core mechanism, Boundary Consistency Regularized Multi-Task Learning (BCRM), enforces prediction agreement between teacher and student models on both segmentation masks and detailed semantic boundaries. To further enhance performance and sharpen contours, BoundMatch incorporates two lightweight fusion modules: Boundary-Semantic Fusion (BSF) injects learned boundary cues into the segmentation decoder, while Spatial Gradient Fusion (SGF) refines boundary predictions using mask gradients, leading to higher-quality boundary pseudo-labels. This framework is built upon SAMTH, a strong teacher-student baseline featuring a Harmonious Batch Normalization (HBN) update strategy for improved stability. Extensive experiments on diverse datasets including Cityscapes, BDD100K, SYNTHIA, ADE20K, and Pascal VOC show that BoundMatch achieves competitive performance against state-of-the-art methods while significantly improving boundary-specific evaluation metrics. We also demonstrate its effectiveness in realistic large-scale unlabeled data scenarios and on lightweight architectures designed for mobile deployment.

**Keywords** Semantic Segmentation · Semi-Supervised Learning · Boundary Detection

## 1 Introduction

Semantic segmentation, the task of assigning a class label to every pixel, provides the detailed scene understanding crucial for many modern vision systems. It is particularly vital for autonomous driving, where precise identification of road boundaries, pedestrians, and vehicles is paramount for safe navigation [1, 2]. Beyond driving, it empowers robotic agents to interact intelligently with complex environments [3, 4], aids in clinical diagnostics through medical image analysis [5, 6], and enables large-scale environmental monitoring via remote sensing [7]. However, the reliance of high-performance models on vast amounts of dense, pixel-level annotations presents a major bottleneck, as manual labeling is extremely time-consuming and costly. Semi-supervised semantic segmentation (SS-SS) offers a compelling solution by aiming to achieve strong performance

while drastically reducing annotation requirements, primarily leveraging large quantities of readily available unlabeled data.

Among various SS-SS strategies, Consistency Regularization (CR) has proven highly effective and is widely adopted, often implemented within teacher-student frameworks [8, 9]. In this setup, a “teacher” model (e.g., an EMA of the “student”) generates pseudo-labels on weakly perturbed unlabeled images, which then supervise the student model trained on strongly perturbed versions of the same images. This encourages the model to learn robust representations invariant to nuisances. While CR methods have significantly boosted overall segmentation accuracy (e.g., mIoU), they tend to focus on improving predictions for interior regions. Consequently, a critical challenge persists: the accurate delineation of object boundaries, which often remain imprecise. This limitation hinders reliability of downstream tasks by adding uncertainty (e.g. a pedestrian merging into the background). Notably, state-of-the-art fully

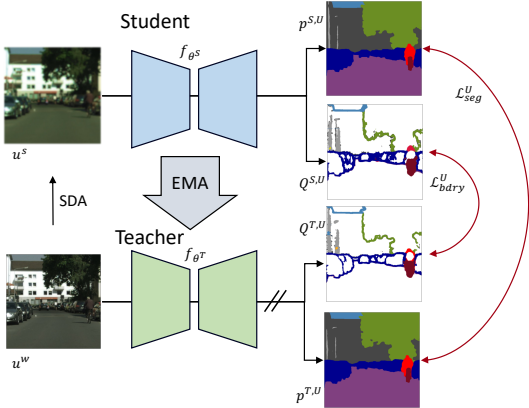


Figure 1: BoundMatch applies consistency regularization (CR) to both segmentation masks and boundaries in semi-supervised semantic segmentation (SS-SS). Its core mechanism, Boundary Consistency Regularized Multi-Task Learning (BCRM), enforces this by “matching” the student’s boundary predictions derived from strongly augmented inputs against boundary pseudo-labels generated by the teacher from weakly augmented inputs. To further enhance performance, lightweight fusion modules refine the teacher’s initial segmentation and boundary predictions, leading to higher-quality pseudo-labels.

supervised methods increasingly address this by incorporating boundary detection as an auxiliary multi-task learning (MTL) objective, yielding demonstrably sharper results [10, 11, 12].

Leveraging boundary information within the semi-supervised setting, however, remains largely underexplored. The few existing attempts either use boundary cues derived from segmentation pseudo-labels mainly to re-weight the consistency loss near edges [13, 14], or, like BoundaryMatch [15], introduce an auxiliary binary boundary detection task using single-stage features, reporting limited benefits when integrated with a modern CR method. Therefore, a crucial opportunity remains: to simultaneously enforce CR on both segmentation masks and detailed semantic boundary predictions derived from rich hierarchical features, and to explicitly fuse this boundary information back into the segmentation pipeline to create a synergistic learning dynamic within SS-SS.

To fill this gap, we propose **BoundMatch**, a novel teacher–student framework designed to effectively integrate multi-task semantic boundary detection with CR for SS-SS. At its core, BoundMatch introduces Boundary Consistency Regularized Multi-Task Learning (BCRM), a mechanism that uniquely enforces prediction agreement between the teacher and student on both the segmentation masks and the semantic boundary maps extracted from hierarchical backbone features. This ensures consistent learning for regions and contours alike from unlabeled data. To maximize the utility of boundary information, BoundMatch incorporates two efficient fusion modules: Boundary-Semantic Fusion (BSF) injects learned boundary cues into the segmentation decoder, promoting more accurate contour localization in the final masks, while Spatial Gradient Fusion (SGF) refines the boundary predictions themselves by incorporating spatial gradients from the segmentation output, leading to higher-quality boundary pseudo-labels

for the consistency objective. Built upon SAMTH, a strong baseline featuring Harmonious Batch Normalization (HBN) for enhanced stability, BoundMatch’s primary novelty lies in this synergistic boundary-centric consistency and fusion approach. It is also designed to be flexible and potentially combinable with other CR methods.

We validate BoundMatch through extensive experiments on diverse benchmarks including Cityscapes, BDD100K, SYNTHIA, ADE20K, and Pascal VOC. Results demonstrate that our method achieves competitive or state-of-the-art performance while significantly improving boundary-specific metrics. Furthermore, we show its effectiveness in realistic large-scale unlabeled data scenarios and its applicability to lightweight architectures suitable for deployment. Our main contributions are:

- We introduce BoundMatch, the first SS-SS framework to apply consistency regularization to semantic boundaries within a multi-task teacher-student setup, enhanced by novel fusion modules (BSF and SGF) for synergistic learning.
- We present SAMTH, a strong and stable SS-SS baseline incorporating Harmonious Batch Normalization (HBN), which benefits various CR methods.
- We provide comprehensive experimental validation demonstrating BoundMatch’s state-of-the-art potential, significant boundary quality improvements, and practical utility across multiple datasets and realistic settings.

## 2 Related Work

**Semantic Segmentation and Boundary-Aware Strategies.** Semantic segmentation has evolved significantly, progressing from early fully convolutional networks (FCNs) [16] to advanced architectures incorporating multi-scale features [17], attention mechanisms [18], and Transformer-based models [19]. The DeepLabV3+ architecture [20], featuring an encoder-decoder structure and atrous convolutions, remains a popular choice due to its effectiveness in capturing both local and global context. Real-time semantic segmentation has also garnered attention, leading to efficient architectures like BiSeNet [21] and AFFormer [22].

Recognizing that segmentation accuracy is often hindered by imprecise object boundaries, boundary-aware methods have emerged. GSCNN [10] was among the first to achieve significant improvements by incorporating multi-task learning (MTL) of boundaries and segmentation. DecoupleSegNet [23] introduced specialized decoders for boundary and interior regions. Inspired by dedicated boundary detection methods [24, 25, 26], RPCNet [27] proposed an MTL framework integrating both tasks. CSEL [28] employed an affinity learning strategy to further refine segmentation. More recent work has focused on conditioning the backbone features with boundary information, exemplified by STDC [29] and SBCB [11]. MobileSeed [12] extended boundary-aware MTL to lightweight Transformer backbones suitable for mobile deployment. However, the ap-

plication of MTL with semantic boundary detection within the SS-SS context remains largely unexplored, motivating our work.

**Semi-Supervised Semantic Segmentation (SS-SS).** Fully supervised semantic segmentation methods require large amounts of costly pixel-wise annotations. SS-SS aims to mitigate this burden by leveraging abundant unlabeled data alongside a smaller labeled set. Consistency regularization (CR), which encourages models to produce consistent predictions under different input perturbations, is a cornerstone technique in SS-SS [30, 31, 32, 33, 34, 35, 36]. A common implementation involves the mean-teacher framework [8], where an exponential moving average (EMA) of the student model’s weights generates stable pseudo-labels for unlabeled data. CutMix-MT [8] integrated CutMix augmentation to enhance consistency. Subsequent works like AugSeg [37] and iMAS [38] explored stronger augmentation strategies. Other directions include using multiple teachers (DualTeacher [39]), incorporating contrastive learning (ReCo [40], U2PL [41]), and unifying various strong-to-weak perturbation regularizations (UniMatch [9] and its variants [42, 43, 44]). Recently, applying SS-SS principles to Transformer-based architectures has gained traction [45, 46, 47]. Our work builds upon these CR foundations by introducing boundary detection as an auxiliary task, an aspect largely missing in prior SS-SS literature. Recognizing the need to validate SS-SS in diverse, practical scenarios, we also evaluate our approach on lightweight architectures suitable for mobile deployment.

### Boundary-Aware Semi-Supervised Semantic Segmentation.

While most SS-SS methods concentrate on pseudo-label refinement and consistency losses, explicit integration of boundary information remains rare. Graph-BAS<sup>3</sup>Net [5] utilized an edge detection auxiliary task for semi-supervised medical image segmentation. CFCG [13], one of the first approaches for natural images, proposed increasing the consistency loss weight for boundary regions identified from pseudo-label masks as training progresses. BoundaryMatch [15] introduced an auxiliary binary boundary detection task, similar to STDC [29], within an SS-SS framework. More recently, CW-BASS [14] proposed a boundary-aware self-training approach.

Although our work also employs boundary consistency, it differs significantly from BoundaryMatch [15]. We utilize a proven semantic boundary detection MTL approach leveraging hierarchical features [11], rather than binary boundaries from single-stage features. Crucially, we introduce explicit feature fusion mechanisms (BSF and SGF) to ensure the boundary information effectively enhances segmentation. As demonstrated in our experiments, this comprehensive integration yields substantial benefits, whereas BoundaryMatch reported minimal effectiveness from their boundary component in the SS-SS setting. Our work uniquely combines semantic boundary consistency regularization derived from hierarchical features with explicit fusion mechanisms, creating a synergistic approach specifically designed for improving boundary delineation in SS-SS.

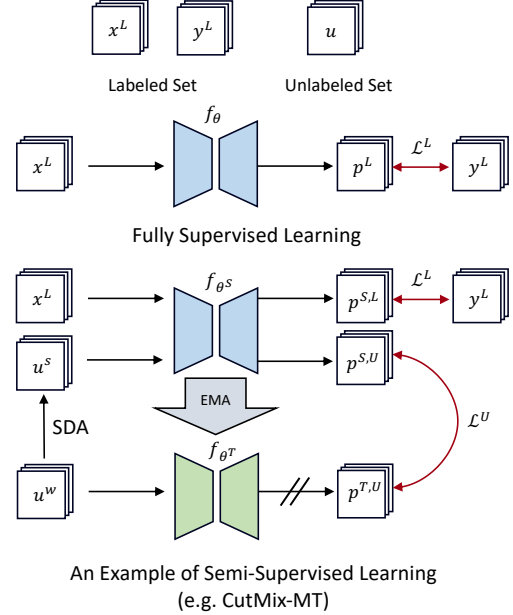


Figure 2: Illustration of the Teacher-Student framework, a common approach for consistency regularization (CR) in semi-supervised semantic segmentation (SS-SS). This framework utilizes unlabeled images by having the teacher model generate pseudo-labels from weakly augmented inputs ( $u^w$ ). These pseudo-labels then supervise the student model, which processes corresponding strongly augmented inputs ( $u^s$ ), thereby enforcing prediction consistency. The teacher model is typically updated via an Exponential Moving Average (EMA) of the student’s weights, and its predictions are detached from the backpropagation graph (indicated by dashed lines).

## 3 Approach

In this section, we present BoundMatch, our multi-task framework that incorporates boundary detection into semi-supervised semantic segmentation (SS-SS). We begin by outlining the notation and preliminaries for SS-SS, including the teacher-student paradigm, in Secs. 3.1 and 3.2. We then introduce SAMTH, our baseline method detailed in Sec. 3.3. Building upon this baseline, Sec. 3.4 describes our core Boundary Consistency Regularized Multi-Task Learning (BCRM) framework. Subsequently, Sec. 3.5 details the complementary boundary-aware modeling and refinement strategies—Boundary-Semantic Fusion (BSF) and Spatial Gradient Fusion (SGF). Finally, Sec. 3.6 synthesizes these components (SAMTH, BCRM, BSF, and SGF) into the complete BoundMatch framework.

### 3.1 Notation and Preliminaries

Let  $\mathcal{D}^L = \{(x_i, y_i)\}_{i=1}^N$  be the labeled dataset, where  $x_i$  denotes the input image and  $y_i \in \{0, 1, \dots, C-1\}^{H \times W}$  represents the corresponding semantic segmentation map with  $C$  semantic classes and spatial dimensions  $H \times W$ . In addition, let  $\mathcal{D}^U = \{u_j\}_{j=1}^M$  be an unlabeled dataset consisting of images  $u_j$ .

The goal of SS-SS is to learn a segmentation model  $f_\theta(\cdot)$  parameterized by  $\theta$  by leveraging both  $\mathcal{D}^L$  and  $\mathcal{D}^U$ . The overall loss is formulated as:

$$\mathcal{L} = \mathcal{L}^L + \lambda \mathcal{L}^U, \quad (1)$$

where  $\mathcal{L}^L$  is the supervised loss over the labeled set and  $\mathcal{L}^U$  is the unsupervised loss applied to the unlabeled set. The pixel-wise cross-entropy loss  $H$  where we can represent the overall supervised loss as:

$$\mathcal{L}^L = \frac{1}{B^L} \sum_{b=1}^{B^L} \frac{1}{HW} \sum_{i,j} H(y^L(b, i, j), p^{S,L}(b, i, j)), \quad (2)$$

with  $p^L = f_\theta(x)$  representing the semantic segmentation prediction for the network.

### 3.2 Teacher–Student Framework for Consistency Regularization

The teacher–student framework, as shown in Fig. 2, is a popular paradigm for SS-SS. It employs consistency regularization (CR) between the predictions of a teacher network and a student network for unlabeled samples. The core idea is to encourage the student network to produce consistent predictions for an unlabeled image under different perturbations. The teacher network, which is typically an exponential moving average (EMA) of the student network, provides more stable and reliable predictions, which are then used to guide the student’s learning.

In our framework, the teacher’s output from weakly augmented images is used to generate hard pseudo-labels that supervise the student’s predictions under strong data augmentation (SDA). This process can be seen as a form of self-distillation, where the student learns from the teacher’s predictions on unlabeled data.

Specifically, given a weakly augmented image  $u^w$  and its strongly augmented counterpart  $u^s$ , we first obtain the teacher’s prediction  $p^{T,w}$  and generate hard pseudo-labels  $\hat{p}^T = \operatorname{argmax}(p^{T,w})$ . These hard pseudo-labels represent the teacher’s most confident predictions for each pixel in the unlabeled image.

The unsupervised consistency loss is then defined as:

$$\mathcal{L}^U = R(p^{S,s}, p^{T,w}) = \frac{1}{B^U} \sum_{b=1}^{B^U} \frac{1}{HW} \sum_{i,j} \mathbf{1}(\max(p^{T,w}(b, i, j)) \geq \tau) H(\hat{p}^T(b, i, j), p^{S,s}(b, i, j)), \quad (3)$$

where  $\mathbf{1}(\cdot)$  is an indicator function, and  $\tau$  is the confidence threshold to filter out noisy pseudo-labels. This loss function measures the discrepancy between the student’s predictions on the strongly augmented unlabeled image and the teacher’s hard pseudo-labels on the weakly augmented version. By minimizing this loss, the student is encouraged to learn from the teacher’s predictions and become more robust to different augmentations.

The student’s parameters are also updated using labeled set via  $\mathcal{L}^L$ . The teacher’s parameters  $\theta^T$  are updated using EMA of

the student’s parameters:

$$\theta^T \leftarrow \alpha \theta^T + (1 - \alpha) \theta^S, \quad (4)$$

with decay rate  $\alpha$ . EMA helps to stabilize the teacher’s predictions by averaging the student’s parameters over time, leading to more reliable pseudo-labels.

### 3.3 Strong Data Augmentation Mean-Teacher with Hard Pseudo-Labels (SAMTH)

Our baseline, SAMTH, builds upon the CutMix-MT framework [8] but distinguishes itself by using hard pseudo-labels, similar to recent methods such as AugSeg [37] and UniMatch [9]. SAMTH leverages CutMix as the strong data augmentation (SDA) to improve the robustness of the student network and the quality of the pseudo-labels.

A key differentiator of SAMTH is its **Harmonious Batch Normalization (HBN)** update strategy, addressing potential instabilities from BN handling in teacher-student frameworks. Common alternatives risk issues: forwarding only partial data through the teacher (e.g., CutMix-MT [8], U2PL [41]) can lead to biased BN statistics unsuitable for the teacher’s full role, while using the student’s BN statistics via copy or EMA (e.g., AugSeg [37], iMAS [38]) couples the teacher’s normalization to the student’s potentially noisy state and risks incompatibility between these borrowed BN statistics and the teacher’s own EMA-updated weights.

HBN mitigates these concerns. We forward the complete batch  $(x, u^w, u^s)$  through both networks:  $p^{S,L}, p^{S,w}, p^{S,s} = f_{\theta^S}(x, u^w, u^s)$  and  $p^{T,L}, p^{T,w}, p^{T,s} = f_{\theta^T}(x, u^w, u^s)$ . Crucially, the teacher’s BN layers remain in `train` mode, updating statistics independently based on the full data stream passing through the teacher’s own parameters. Subsequently, only the teacher’s non-BN weights are updated via EMA. This ensures the teacher’s BN statistics are harmonious with its specific weights and the full input distribution, decoupling its normalization from student fluctuations. This promotes more stable training dynamics and improves performance, as validated empirically across multiple baselines in our ablations (Sec. 4.3.5).

### 3.4 Boundary Consistency Regularized Multi-Task Learning (BCRM)

While many semantic segmentation approaches rely solely on segmentation supervision, recent works have demonstrated the benefit of multi-task learning (MTL) with a boundary detection task. BCRM takes this concept further by applying consistency regularization (CR) to both segmentation and boundary predictions.

#### 3.4.1 Notation and Boundary Detection Head

We adopt a lightweight boundary detection head inspired by SBCB [11] and CASENet [26]. The architecture leverages hierarchical features from the backbone (e.g., features from Stem, layer1, layer2, and layer4 of a ResNet). Features from the earlier layers are processed to yield single-channel outputs, while the layer4 feature produces an output with  $C$  channels,

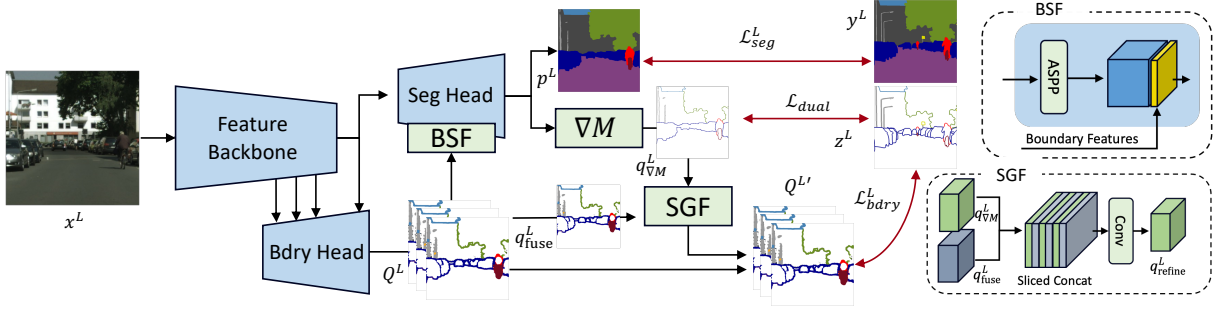


Figure 3: Overview of the BoundMatch architecture processing labeled samples, illustrating multi-task learning (MTL) of boundary detection alongside segmentation. The Boundary-Semantic Fusion (BSF) module integrates learned boundary cues from the boundary head into the segmentation head’s features, promoting sharper segmentation contours. Concurrently, the Spatial Gradient Fusion (SGF) module refines the boundary predictions by fusing them with the spatial gradient of the segmentation mask ( $\nabla M$ ). This refinement improves the quality of boundary supervision for the labeled loss and is crucial for generating cleaner boundary pseudo-labels used in the consistency regularization process for unlabeled data.

where  $C$  is the number of classes. Specifically, the features from these layers are passed through a single  $3 \times 3$  convolutional layer, respectively, each followed by BN and ReLU activation. These processed features are then bilinearly upsampled to the original image size. Following [11], we use an additional  $3 \times 3$  convolutional layer to reduce artifacts from upsampling. The outputs are then fused using a sliced concatenation and undergo a grouped convolution to form the final boundary prediction map of shape  $C \times H \times W$ .

Let  $Q$  denote the set of boundary predictions (e.g., fused output  $q_{\text{fuse}}$  and the layer4 output  $q_{\text{last}}$ ). For the binary boundary detection task, the ground-truth boundary is denoted by  $z$  and the boundary prediction  $q$  is a sigmoid-activated probability map in  $[0, 1]$ . We supervise these outputs using a reweighted pixel-wise binary cross-entropy loss:

$$H_{\text{bdry}}(z, q) = \beta(1 - z) \log(1 - q) + (1 - \beta)z \log(q), \quad (5)$$

where the weights are defined by  $\beta = |z^+|/|z|$ ,  $1 - \beta = |z^-|/|z|$ , with  $|z^+|$  and  $|z^-|$  representing the number of boundary and non-boundary pixels, respectively. This reweighting addresses the class imbalance between boundary and non-boundary pixels, ensuring that the model effectively learns to detect boundaries.

For semantic (multi-label) boundaries, we use a reweighted multi-label cross-entropy loss over the  $C$  channels. The supervised boundary loss is then given by:

$$\mathcal{L}_{\text{bdry}}^L = \sum_{q \in Q^L} \frac{1}{BL} \sum_{b=1}^{B^L} \frac{1}{CHW} \sum_{c,i,j} H_{\text{bdry}}(z(b, c, i, j), q(b, c, i, j)). \quad (6)$$

While our primary auxiliary task is semantic boundary detection, we also explore the use of binary boundaries in Sec. 4.3.2. We opt for semantic boundaries because they provide richer, class-specific edge information compared to generic binary edges. This detailed supervision can encourage the model to learn features that better distinguish between adjacent classes, potentially leading to improved feature representations in the backbone [11].

### 3.4.2 MTL for SS-SS with Boundaries

For the labeled set, the boundary detection head is trained alongside the segmentation head. For unlabeled data, we perform consistency regularization analogous to segmentation as shown in Fig. 1. The teacher’s fused boundary is used to obtain a hard pseudo-label with threshold  $\tau_{\text{bdry}}$ :  $\hat{q}^T = \mathbf{1}(q^{T,w} \geq \tau_{\text{bdry}})$ . The unsupervised boundary loss is then:

$$\mathcal{L}_{\text{bdry}}^U = \sum_{q \in Q^U} \frac{1}{B^U} \sum_{b=1}^{B^U} \frac{1}{CHW} \sum_{c,i,j} H_{\text{bdry}}(\hat{q}^T(b, c, i, j), q^{S,s}(b, c, i, j)). \quad (7)$$

## 3.5 Boundary-Aware Modeling and Refinement

To further enhance the boundary quality and boost segmentation performance, we propose two complementary modules: **Boundary-Semantic Fusion (BSF)** and **Spatial Gradient Fusion (SGF)**. BSF and SGF are simple yet effective mechanisms that refine the boundary and segmentation predictions by incorporating boundary cues and spatial gradients as shown in Fig. 3.

### 3.5.1 Boundary-Semantic Fusion (BSF)

Inspired by GSCNN [10], BSF explicitly integrates boundary predictions into the segmentation head. The output from the boundary detection head is concatenated with the features from the Atrous Spatial Pyramid Pooling (ASPP) using the bottleneck layer of the DeepLabV3+ decoder. We emphasize that there are no extra layers introduced by BSF, and we only add extra channels for the bottleneck layer. This explicit incorporation of boundary cues helps localize object contours more accurately in the final segmentation.

### 3.5.2 Spatial Gradient Fusion (SGF)

Semantic boundary detection may suffer from coarse predictions. To refine the boundaries, we adopt the spatial gradient operator as in RPCNet [27]. The spatial gradient of the semantic mask  $M$  is computed as:

$$\nabla M(i, j) = \|M(i, j) - \text{pool}(M(i, j))\|, \quad (8)$$

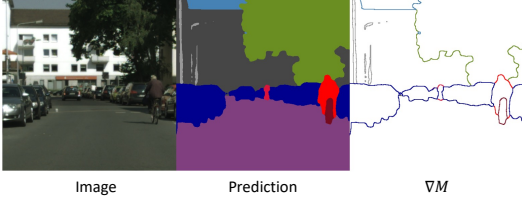


Figure 4: Visualization of the output of spatial gradient operator on segmentation prediction. The produced mask  $\nabla M$  is clean, but instance insensitive boundaries.

where pool denotes adaptive average pooling with a  $3 \times 3$  kernel. An example of the spatial gradient operator is shown in Fig. 4. The resulting gradient map,  $q_{\nabla M}$ , is concatenated with the boundary prediction  $q_{\text{fuse}}$  for each channel:

$$[q_{\text{fuse},1}, q_{\nabla M,1}, q_{\text{fuse},2}, q_{\nabla M,2}, \dots, q_{\text{fuse},C}, q_{\nabla M,C}], \quad (9)$$

forming a  $2C$ -channel activation map. This map is then processed by a convolutional layer with  $C$ -grouped convolutions to yield a refined semantic boundary probability map  $q_{\text{refine}}$ . This grouped convolution refines the boundary predictions by considering the spatial gradients, effectively sharpening the boundaries between different semantic regions.

The refined boundaries are supervised using the same  $H_{\text{bdry}}$  loss. Moreover, we introduce a duality loss on the labeled set to enforce consistency between the spatial gradient and the ground-truth boundaries:

$$\mathcal{L}_{\text{dual}} = \frac{1}{B^L} \sum_{b=1}^{B^L} \frac{1}{CHW} \sum_{c,i,j} |q_{\nabla M}^L(b,c,i,j) - z(b,c,i,j)|. \quad (10)$$

We apply the duality loss only on labeled samples because the ground-truth boundary annotations are reliable; applying it on unlabeled data, which relies on pseudo-labels, introduces instability.

### 3.6 BoundMatch

Finally, BCRM combined with BSF and SGF forms the **BoundMatch** framework. The labeled and unlabeled losses when we apply BoundMatch to SAMTH (SAMTH+BoundMatch) is

$$\mathcal{L}^L = \mathcal{L}_{\text{seg}}^L + \lambda_{\text{bdry}} \mathcal{L}_{\text{bdry}}^L + \lambda_{\text{dual}} \mathcal{L}_{\text{dual}}, \quad (11)$$

$$\mathcal{L}^U = \lambda_{\text{seg}} \mathcal{L}_{\text{seg}}^U + \lambda_{\text{bdry}} \mathcal{L}_{\text{bdry}}^U, \quad (12)$$

and the total loss is

$$\mathcal{L} = \mathcal{L}^L + \lambda \mathcal{L}^U. \quad (13)$$

Although demonstrated primarily with our SAMTH baseline throughout the experiments, BoundMatch is designed to be flexible and compatible with various CR methods. For instance, BoundMatch can be integrated with UniMatch [9] by incorporating the boundary consistency loss alongside UniMatch’s existing feature-level and strong-view consistency losses. We observed that using only a single model (without a teacher) tends to generate noisy boundary pseudo-labels; therefore, employing an EMA-updated teacher model is crucial for stability and quality. Similarly, integration with PrevMatch [42] is

achieved by computing the boundary consistency loss using its robust ensemble pseudo-labels, thereby circumventing potential instability associated with single-iteration predictions. Furthermore, the architectural simplicity of the BSF and SGF fusion modules facilitates the incorporation of BoundMatch’s boundary-enhancement components into diverse segmentation models, a versatility explored in our ablation studies.

## 4 Experiments

In this section, we validate our proposed approach, BoundMatch, through comprehensive experiments. We first benchmark BoundMatch against recent state-of-the-art SS-SS methods on several benchmark datasets. Subsequently, we present detailed ablation studies to analyze the individual contributions of our core components (BCRM, BSF, SGF), evaluate the effect of the chosen boundary formulation (semantic vs. binary), and assess the impact of our Harmonious Batch Normalization (HBN) update strategy. Finally, we report the computational cost associated with BoundMatch and applications to more real-world settings.

### 4.1 Experimental Configuration

Here, we specify the experimental configuration used for evaluating BoundMatch. This includes the datasets utilized (covering urban scenes and standard SS-SS academic benchmarks), the model architectures, and key implementation details.

#### 4.1.1 Datasets

We primarily evaluate our method on urban scene datasets, including Cityscapes, BDD100K, and SYNTHIA, while also considering Pascal VOC 2012 and ADE20K to assess performance in more diverse scenarios. In all semi-supervised learning protocols, the images not selected as labeled data form the unlabeled set for training.

**Cityscapes dataset** [1] is tailored for semantic understanding of urban street scenes. It comprises 2,975 high-resolution training images and 500 validation images, with annotations for 19 semantic categories. In our experiments, we follow the splits defined by UniMatch [9] and evaluate on label partitions corresponding to  $1/16$ ,  $1/8$ , and  $1/4$  of the full labeled training set.

**BDD100K dataset** [48], originally designed for multi-task learning in autonomous driving, contains 100,000 video frames. For our segmentation experiments, we utilize a subset of 8,000 images ( $1280 \times 720$  resolution), divided into 7,000 for training and 1,000 for validation. As BDD100K has not been widely used previously for SS-SS evaluation, we define labeled splits corresponding to  $1/64$ ,  $1/32$ , and  $1/16$  of the available training annotations.

**SYNTHIA dataset** [49] provides synthetic urban scenes generated via computer graphics. We utilize the SYNTHIA-RAND ("Rand") subset, containing 13,400 images ( $1280 \times 760$  resolution) with annotations aligned to the Cityscapes semantic categories. For our experiments, we use a split of 7,000 train-

ing images and 1,000 validation images, evaluating on labeled partitions corresponding to  $1/64$ ,  $1/32$ , and  $1/16$ .

**PASCAL VOC 2012** [50] is a standard object recognition benchmark consisting of 10,582 images annotated for 21 classes (20 object categories plus background). Following established SS-SS protocols, we consider two training settings: the ‘‘Classic’’ protocol uses only the high-quality subset of 1,464 images for the labeled pool, while the ‘‘Blender’’ protocol samples labeled images randomly from the entire dataset.

**ADE20K dataset** [51] offers diverse scenes with dense annotations covering 150 semantic categories. It includes 20,210 training images and 2,000 validation images. Following prior work, we evaluate on label partitions of  $1/128$ ,  $1/64$ , and  $1/32$  of the training set.

#### 4.1.2 Implementation Details

Our experiments utilize ResNet-50 and ResNet-101 as encoder backbones across all datasets, coupled with a DeepLabV3+ segmentation head using an output stride of 16 for training efficiency. For generating semantic and binary boundary labels, we employ the on-the-fly (OTF) strategy from [11]. This approach integrates boundary extraction into the data loading pipeline, guaranteeing consistent boundary widths despite random resizing augmentations.

Key hyperparameters are configured per dataset group:

**Cityscapes, BDD100K, SYNTHIA:** We use a base learning rate of 0.01. Loss weights are set to  $\lambda_{seg} = 1.0$ ,  $\lambda_{bdry} = 0.5$ ,  $\lambda_{dual} = 1.0$ , with an overall unsupervised loss weight  $\lambda = 1.0$ . The EMA decay is  $\alpha = 0.99$ , and the confidence threshold for segmentation pseudo-labels is  $\tau = 0$ . Training uses a mini-batch size of 16 (8 labeled, 8 unlabeled) for 80,000 iterations. The input crop size is  $801 \times 801$  for Cityscapes and  $641 \times 641$  for BDD100K and SYNTHIA.

**Pascal VOC:** Hyperparameters are adjusted: base learning rate is 0.001, boundary loss weight  $\lambda_{bdry} = 0.1$ , duality loss weight  $\lambda_{dual} = 0.5$  (other weights remain  $\lambda_{seg} = 1.0$ ,  $\lambda = 1.0$ ). EMA decay is increased to  $\alpha = 0.999$ , and the segmentation confidence threshold is raised to  $\tau = 0.95$ . We use a mini-batch size of 32 (16 labeled, 16 unlabeled) and train for 120,000 iterations with a  $321 \times 321$  crop size.

**ADE20K:** We adopt the same loss weights ( $\lambda_{seg}, \lambda_{bdry}, \lambda_{dual}, \lambda$ ), EMA decay ( $\alpha$ ), and segmentation threshold ( $\tau$ ) as used for Pascal VOC. However, specific training parameters differ: the base learning rate is 0.01, mini-batch size is 16 (8 labeled, 8 unlabeled), training duration is 80,000 iterations, and the input crop size is  $513 \times 513$ .

Training employs the stochastic gradient descent (SGD) optimizer with a polynomial learning rate decay scheduler. Image augmentations follow UniMatch practices [9], combining weak transformations (resizing, random cropping, horizontal flipping) with strong augmentations (color jittering, grayscale conversion, Gaussian blurring, CutMix). To stabilize the unsupervised loss components, we apply a sigmoid ramp-up schedule:  $\lambda_{seg}$  increases from 0 to its target value over the first 15% of

Table 1: Comparison with recent state-of-the-art methods on the Cityscapes dataset. All methods are trained using ResNet-50/101 and DeepLabV3+. For our methods, we averaged over three runs. The evaluation metric is the mIoU (%).

Cityscapes	ResNet-50			ResNet-101		
	$1/16$	$1/8$	$1/4$	$1/16$	$1/8$	$1/4$
Supervised	63.3	70.2	73.1	66.3	72.8	75.0
U2PL [41] [CVPR'22]	70.6	73.0	76.3	70.3	74.4	76.5
CVCC [32] [CVPR'23]	74.9	76.4	77.3	-	-	-
iMAS [38] [CVPR'23]	74.3	77.4	78.1	-	-	-
AugSeg [37] [CVPR'23]	73.7	76.5	78.8	75.2	77.8	79.6
UniMatch [9] [CVPR'23]	75.0	76.8	77.5	76.6	77.9	79.2
LogicDiag [53] [ICCV'23]	-	-	-	76.8	78.9	<b>80.2</b>
CSS [54] [ICCV'23]	-	-	-	74.0	76.9	77.9
Co-T. [55] [ICCV'23]	-	76.3	77.1	75.0	77.3	78.7
DAW [56] [NeurIPS'23]	75.2	77.5	79.1	76.6	78.4	79.4
CorrMatch [33] [CVPR'24]	-	-	-	77.3	78.5	79.4
RankMatch [34] [CVPR'24]	75.4	77.7	<u>79.2</u>	77.1	78.6	80.0
DDFP [35] [CVPR'24]	-	-	-	77.1	78.2	79.9
PrevMatch [42] [ArXiv'24]	75.8	77.8	78.8	<u>77.7</u>	<u>78.9</u>	<u>80.1</u>
UCCL [36] [ICASSP'25]	75.8	77.2	78.2	-	-	-
NRCR [43] [NN'25]	-	77.0	77.9	-	78.2	79.5
DMSI [44] [TMM'25]	75.9	<b>78.0</b>	<u>79.2</u>	77.0	<b>79.0</b>	79.8
CW-BASS [14] [ArXiv'25]	75.0	77.2	78.4	-	-	-
SAMTH	<u>75.1</u>	<u>77.3</u>	<u>78.9</u>	75.5	77.9	<u>79.7</u>
SAMTH+BoundMatch	<b>76.5</b>	<u>77.9</u>	<b>79.3</b>	<b>77.9</b>	<b>79.0</b>	<u>80.1</u>

iterations, while  $\lambda_{bdry}$  ramps up linearly throughout the entire training process.

All experiments are implemented using PyTorch and the msegmentation library [52]. Training is conducted on dual-GPU setups, using either two NVIDIA RTX 3090 or two NVIDIA A6000 GPUs, depending on the memory footprint of the specific benchmark and model configuration.

## 4.2 Comparisons with State-of-the-Art Methods

### 4.2.1 Cityscapes

Tab. 1 summarizes the quantitative results on the Cityscapes dataset across various labeled data splits ( $1/16$ ,  $1/8$ ,  $1/4$ ) for both ResNet-50 and ResNet-101 backbones. Compared with recent state-of-the-art methods, SAMTH+BoundMatch achieves significant performance improvements, particularly in the low-data regime. Notably, incorporating the boundary-aware components allows SAMTH+BoundMatch to consistently outperform the SAMTH baseline, yielding mIoU gains ranging from 1.4% to 2.6% across the tested settings. We attribute this improvement, especially pronounced with limited labeled data, to the additional regularization provided by the boundary multi-task learning objective, as strong regularization techniques are often particularly effective in low-supervision scenarios. The qualitative results presented in Fig. 5 further illustrate that SAMTH+BoundMatch produces more precise object boundaries and improves segmentation accuracy for challenging classes such as ‘‘wall’’, ‘‘pole’’, ‘‘train’’, and ‘‘bus’’. Overall, these findings establish SAMTH as a strong baseline for urban scene SS-SS, while SAMTH+BoundMatch demonstrates competitive performance against state-of-the-art methods through its effective integration of boundary awareness.

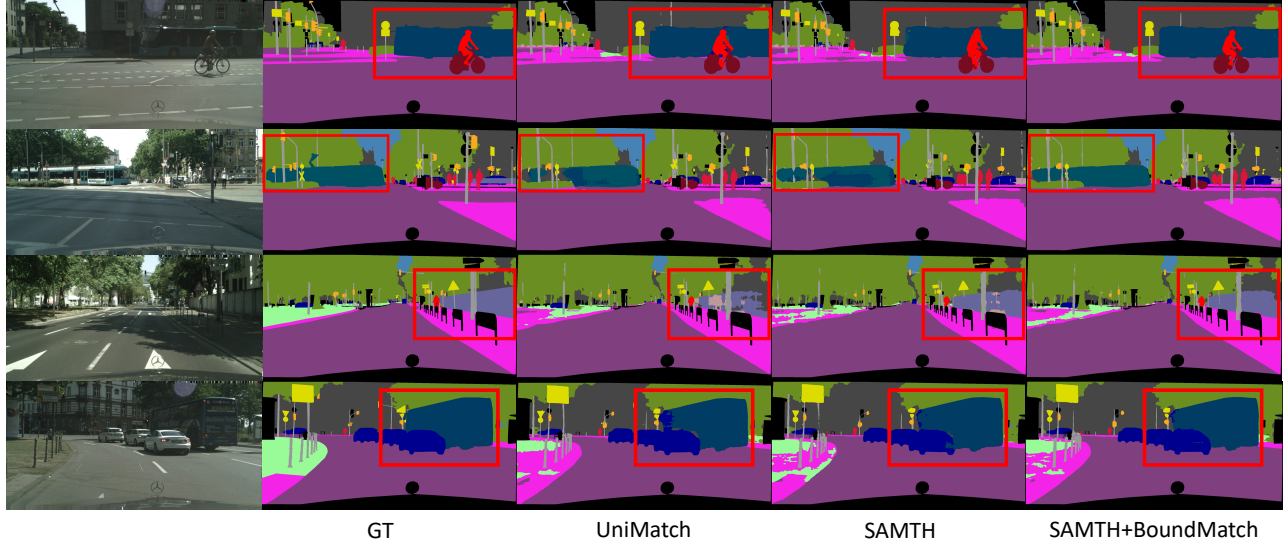


Figure 5: Qualitative results on the Cityscapes dataset on  $1/16$  split. We compare UniMatch [9] with our SAMTH baseline and SAMTH+BoundMatch. Our method produces less segmentation errors especially for object boundaries and difficult categories. Best viewed zoomed in and in color.

Table 2: Comparison with our method (SAMTH+BoundMatch) against UniMatch and PrevMatch on the BDD100K, SYNTHIA, and ADE20K datasets. All methods use DeepLabV3+ with ResNet-50 backbone.

Method	BDD100K			SYNTHIA			ADE20K		
	$1/64$	$1/32$	$1/16$	$1/64$	$1/32$	$1/16$	$1/128$	$1/64$	$1/32$
Supervised	40.4	45.3	52.1	63.3	78.5	69.7	7.2	9.9	13.7
UniMatch [9]	49.2	52.3	56.4	68.5	71.9	72.4	13.6	18.3	23.9
PrevMatch [42]	-	-	-	-	-	-	15.4	<b>19.6</b>	24.9
Ours	<b>52.4</b>	<b>53.9</b>	<b>57.8</b>	<b>69.9</b>	<b>73.0</b>	<b>74.8</b>	<b>15.6</b>	<b>19.6</b>	<b>25.3</b>

#### 4.2.2 BDD100K, SYNTHIA, and ADE20K

To assess the generalizability of our approach, we extended the evaluation to additional datasets: the urban driving scene datasets BDD100K and SYNTHIA, as well as the challenging academic benchmark ADE20K, known for its diversity and difficulty in semantic segmentation. As shown in Tab. 2, SAMTH+BoundMatch consistently yields significant improvements over supervised baselines and UniMatch on these datasets. For instance, on BDD100K, our method improves the mean IoU by over 2% for the  $1/64$  split. On the complex ADE20K dataset, our method is competitive against the capable PrevMatch. These results demonstrate that our boundary-aware learning framework effectively leverages unlabeled data across various domains, including challenging datasets with complex scenes.

#### 4.2.3 Pascal VOC 2012

We further evaluate our method on the Pascal VOC 2012 dataset using both the *Classic* and *Blender* splits, acknowledging the challenges posed by this benchmark.

**Classic Split:** Tab. 3 presents the performance comparison on the Classic splits for both ResNet-50 and ResNet-101 backbones. It is important to note that Pascal VOC 2012 boundary annotations are known to be noisy, and boundary regions are

Table 3: Comparison with recent state-of-the-art methods on the Pascal VOC 2012 dataset using the *Classic* splits. All methods are trained using ResNet-50/101 and DeepLabV3+.

Classic	ResNet-50			ResNet-101		
	92	183	366	92	183	366
Supervised	44.0	52.3	61.7	45.1	55.3	64.8
CVCC [32] [CVPR'23]	-	-	-	70.2	74.4	77.4
iMAS [38] [CVPR'23]	-	-	-	68.8	74.4	78.5
AugSeg [37] [CVPR'23]	64.2	72.2	76.2	71.1	75.5	78.8
UniMatch [9] [CVPR'23]	71.9	72.5	76.0	75.2	77.2	78.8
ESL [57] [ICCV'23]	-	69.5	72.6	71.0	74.1	78.1
CSS [54] [ICCV'23]	68.0	71.9	74.9	-	-	-
Co-T. [55] [ICCV'23]	73.1	74.7	77.1	75.7	77.7	<b>80.1</b>
DAW [56] [NeurIPS'23]	68.5	73.1	76.3	74.8	77.4	79.5
CorrMatch [33] [CVPR'24]	-	-	-	76.4	78.5	79.4
RankMatch [34] [CVPR'24]	71.6	74.6	76.7	75.5	77.6	79.8
PrevMatch [42] [ArXiv'24]	73.4	<b>75.4</b>	<b>77.5</b>	77.0	78.5	79.6
NRCL [36] [ICASSP'25]	-	74.1	77.1	-	-	-
NRCR [43] [NN'25]	-	-	-	<b>77.4</b>	<b>79.7</b>	<b>80.2</b>
DMSI [44] [TMM'25]	-	-	-	76.5	77.4	79.7
CW-BASS [14] [ArXiv'25]	72.8	<b>75.8</b>	76.2	-	-	-
SAMTH+BoundMatch	72.6	<b>73.8</b>	<b>77.3</b>	76.6	<b>78.3</b>	78.9
UniMatch+BoundMatch	<b>74.2</b>	<b>75.8</b>	76.9	76.0	78.2	78.9
PrevMatch+BoundMatch	<b>74.5</b>	<b>75.8</b>	<b>77.7</b>	<b>77.2</b>	<b>78.7</b>	79.7

typically treated as “ignore labels” during training and evaluation. While SAMTH+BoundMatch improves performance relative to earlier CR methods like AugSeg and UniMatch, it does not reach the state-of-the-art results achieved by the most recent approaches, such as PrevMatch and CW-BASS, on this dataset. We hypothesize this performance gap is partly attributable to the weak CR approach of SAMTH, making it less effective for this dataset. To further assess BoundMatch’s boundary mechanism independently of our SAMTH baseline, we integrated it with established CR methods: UniMatch and PrevMatch. When combined with these strong baselines, BoundMatch consistently yields mean IoU gains over the original methods, achieving results that are competitive with, or reach, current state-of-the-art performance (Tab. 3).

**Blended Split:** This split contains potentially even more noisy GT labels, particularly around object boundaries. Tab. 4 shows

Table 4: Comparison with recent state-of-the-art methods on the Pascal VOC 2012 dataset using the *Blender* splits. All methods are trained using ResNet-50 and DeepLabV3+.

Blender		1/16	1/8	1/4
Supervised		62.4	68.2	72.3
CVCC [32]	[CVPR'23]	74.5	76.1	76.4
iMAS [38]	[CVPR'23]	74.8	76.5	77.0
AugSeg [37]	[CVPR'23]	74.7	76.0	77.2
UniMatch [9]	[CVPR'23]	75.8	76.9	76.8
CFCG [13]	[ICCV'23]	75.6	77.6	78.3
DAW [56]	[NeurIPS'23]	<u>76.2</u>	77.6	77.4
RankMatch [34]	[CVPR'24]	<b>76.6</b>	77.8	78.3
PrevMatch [42]	[ArXiv'24]	76.0	77.1	77.6
IpxMatch [58]	[IJCNN'24]	74.5	74.9	75.0
NRCR [43]	[NN'25]	<b>76.6</b>	<b>78.2</b>	78.7
DMSI [44]	[TMM'25]	75.5	75.3	75.9
SAMTH+BoundMatch		76.0	77.2	77.9
UniMatch+BoundMatch		<b>76.6</b>	77.9	<b>78.9</b>
PrevMatch+BoundMatch		<b>76.6</b>	77.8	78.0

Table 5: Component Analysis.

BCRM	BSF	SGF	IoU	BIoU	BF1
			75.06	54.93	59.50
✓			75.91	55.25	60.22
✓	✓		76.21	55.95	61.97
✓		✓	76.10	55.70	61.64
✓	✓	✓	76.38	55.97	62.46

trends similar to the Classic split. Again, the combinations of BoundMatch with UniMatch or PrevMatch achieve performance competitive with recent SOTA methods. Notably, BoundMatch variants (including SAMTH+BoundMatch and its combinations with UniMatch/PrevMatch) generally outperform CFCG [13], another SS-SS method that utilizes boundary information.

Collectively, these Pascal VOC results underscore the benefit of incorporating explicit boundary modeling in SS-SS frameworks. They demonstrate advantages even when reliant on datasets with imperfect boundary annotations, particularly when BoundMatch’s components enhance already strong CR baselines.

### 4.3 Ablation Studies and Insights

In this section, we conduct ablation studies to analyze the impact of each proposed component and design choice. We report results on the Cityscapes dataset under the 1/16 labeled data split (unless explicitly stated), and our evaluation metrics include the mean Intersection-over-Union (IoU), boundary IoU (BIoU), and boundary F1 score (BF1).

#### 4.3.1 Individual efficacy of the proposed components

Tab. 5 reports the quantitative results for various combinations of our proposed components, starting from the SAMTH baseline which lacks explicit boundary supervision. The addition of our core BCRM framework alone results in notable gains in both segmentation and boundary quality metrics. Further incorporating the BSF module builds upon this, enhancing performance by effectively integrating learned boundary cues into the segmentation head. Finally, adding the SGF module pro-

Table 6: Binary vs. Multi-Label Boundaries.

	IoU	BIoU	BF1
SAMTH	75.06	54.93	59.50
+Binary	75.90	55.38	60.10
+Multi-Label	76.38	55.97	62.46

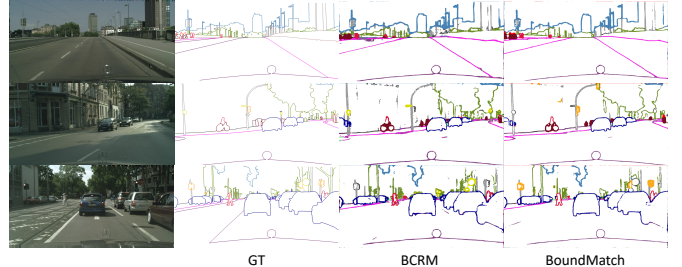


Figure 6: Qualitative comparison illustrating the impact of Spatial Gradient Fusion (SGF) on boundary predictions (Cityscapes dataset, 1/16 split). Boundaries generated using only the BCRM component tend to be thicker and contain more artifacts (false positives). In contrast, the full BoundMatch framework, incorporating the SGF module, produces visibly sharper and cleaner boundaries. SGF achieves this by refining the initial boundary predictions, leveraging spatial gradient information derived from the segmentation mask. This refinement process is crucial for generating higher-quality boundary pseudo-labels, subsequently enhancing the effectiveness of the CR. Best viewed in color and zoomed in.

vides complementary benefits; its strategy of refining boundary predictions using spatial gradients derived from the segmentation mask leads to the highest overall performance observed in our ablation.

#### 4.3.2 Binary vs Semantic Boundaries

An important design decision in our method is whether to model boundaries as binary or multi-label (semantic). As shown in Tab. 6, while both formulations improve upon the SAMTH baseline, the semantic boundary formulation achieves the highest improvement in segmentation performance (with IoU increasing from 75.06% to 76.38%). Performance gains from semantic boundaries are supported by experiments in the fully supervised setting for urban scene segmentation [11]. We believe this forces the model to learn not just geometric structures but also semantic context of the boundaries. This suggests that incorporating semantic context into the boundary predictions allows the network to better differentiate between object classes at the boundaries.

#### 4.3.3 Boundary Evaluation

Qualitative evaluations of the boundary predictions are presented in Fig. 6. We observe that the proposed multi-label boundary formulation yields sharper and more precise object contours compared to the baseline and binary boundary formulations. These qualitative results corroborate the quantitative improvements reported in the previous subsections.

While mIoU remains the de facto standard for assessing overall segmentation quality, it is well known to be insensitive to errors occurring specifically at object contours [10, 59]. To explicitly quantify boundary fidelity, we adopt two complementary metrics: **Boundary IoU (BIOU)** and **Boundary F1 Score (BF1)**.

**Boundary IoU (BIOU):** BIOU evaluates the overlap between predicted ( $\hat{y}$ ) and ground-truth segmentation masks  $y$  restricted only to pixels lying within a narrow-band around object boundaries. Formally, BIOU is computed as

$$\text{BIOU} = \frac{1}{C} \sum_{c=1}^C \frac{\sum_n \sum_{(i,j) \in \text{BD}(y_n)} [\hat{y}_{n,c,i,j} \wedge y_{n,c,i,j}]}{\sum_n \sum_{(i,j) \in \text{BD}(y_n)} [\hat{y}_{n,c,i,j} \vee y_{n,c,i,j}]}, \quad (14)$$

where  $\text{BD}(y) = y \oplus \text{MinPool}(y)$  denotes the binary boundary mask obtained by applying a  $3 \times 3$  min-pooling (stride 1) to the ground-truth segmentation map  $y$  and taking the pixel-wise XOR ( $\oplus$ ) with the original mask, and  $\wedge$  and  $\vee$  denote pixel-wise logical AND and OR, respectively [60]. Because it ignores interior pixels, BIOU directly measures contour alignment and penalizes both over- and under-segmentation along object edges. It is therefore particularly sensitive to boundary precision but agnostic to interior region accuracy. We use a 5 pixel radius for the boundary mask in our experiments.

**Boundary F1 Score (BF1):** In contrast, BF1 captures both boundary precision (the fraction of predicted boundary pixels that lie near a true boundary) and recall (the fraction of true boundary pixels recovered by the prediction), combining them via the harmonic mean:

$$\text{BF1} = \frac{1}{C} \sum_{c=1}^C \frac{2 \text{Prec}_c \text{Rec}_c}{\text{Prec}_c + \text{Rec}_c}, \quad (15)$$

where precision and recall are computed by matching predicted and ground-truth boundary pixels within a small tolerance radius [61]. Formally, precision and recall can be defined as:

$$\text{Prec}_c = \frac{\sum_{n,h,w} [\text{BD}(\hat{y}_n)_{c,h,w} \wedge \text{MaxPool}(\text{BD}(y_n))_{c,h,w}]}{\sum_{n,h,w} \text{BD}(\hat{y}_n)_{c,h,w}}, \quad (16)$$

and

$$\text{Rec}_c = \frac{\sum_{n,h,w} [\text{MaxPool}(\text{BD}(\hat{y}_n))_{c,h,w} \wedge \text{BD}(y_n)_{c,h,w}]}{\sum_{n,h,w} \text{BD}(y_n)_{c,h,w}}. \quad (17)$$

BF1 thus provides insight into the trade-off between missing fine boundary details (low recall) and producing spurious edges (low precision), while allowing for minor spatial misalignments. We use a 5 pixel tolerance radius for our experiments.

**Complementary Insights:** BIOU emphasizes exact contour overlap, making it well suited for tasks requiring crisp, well-aligned boundaries. BF1, by explicitly balancing precision and recall under a spatial tolerance, is more robust to slight shifts but sensitive to fragmented or noisy boundary predictions. Reporting both metrics alongside mIoU therefore provides a holistic view of a model’s segmentation performance, particularly its ability to delineate object contours accurately.

Table 7: Comparison between our BoundMatch method and BoundaryMatch. Performance values for UniMatch [9] and BoundaryMatch [15] are included for context. For BoundaryMatch, we also reimplemented their method and trained the method with the same setting for fairness. All methods use ResNet-101 as the backbone.

Methods	VOC (92)	City. ( $1/16$ )
UniMatch	75.2	76.6
BoundaryMatch	75.4	76.0
BoundaryMatch (reproduced)	75.5	76.8
SAMTH+BoundMatch	76.6	77.9
UniMatch+BoundMatch	76.0	77.4

**Analysis of BIOU and BF1 Scores:** Tab. 5 and Tab. 6 reports the BIOU and BF1 scores for various configurations of our proposed components and boundary types. We observe that the addition of boundary-aware components (BCRM, BSF, and SGF) consistently improves both BIOU and BF1 scores, with BSF and SGF having similar gains. Combining the two components results in a significant boost compared to BCRM, with the highest boundary metrics. We also found that Binary boundaries are less effective than Multi-Label boundaries, which is consistent with the segmentation results. These improvements in BIOU and BF1 underscore the effectiveness of our approach in capturing fine-grained boundary details. The refined boundaries contribute not only to visually sharper segmentation maps but also to more accurate delineation of object contours, which is critical for applications requiring precise localization.

#### 4.3.4 Comparisons with BoundaryMatch

We compared our BoundMatch approach against BoundaryMatch [15], a recent method that also utilizes boundary CR for SS-SS. For a fair comparison based on our experimental setup, we reimplemented BoundaryMatch and trained it using identical settings. Quantitative results are presented in Tab. 7.

While BoundaryMatch shows minor gains over its UniMatch baseline, our SAMTH+BoundMatch method significantly outperforms the reproduced BoundaryMatch implementation by 1.1% mIoU on both Pascal VOC (92 split) and Cityscapes ( $1/16$  split). Furthermore, integrating BoundMatch’s principles with UniMatch (UniMatch+BoundMatch) also surpasses BoundaryMatch’s performance on both datasets, although the improvement margin is larger when using our SAMTH baseline, suggesting potential synergy effects.

We attribute BoundMatch’s superior performance to its more comprehensive handling of boundary information. Specifically, our method employs: (1) *semantic* boundary supervision, providing richer class-specific edge cues compared to binary boundaries; (2) boundary heads leveraging *hierarchical features* from the backbone with *deep supervision*, known to be effective for capturing crucial multi-scale boundary details [26]; and (3) dedicated *fusion modules* (BSF, SGF) that integrate boundary information back into the segmentation process and refine boundary predictions. In contrast, the BoundaryMatch approach utilizes binary boundaries derived from only a single backbone feature stage. This suggests that simpler boundary consistency regularization might not fully exploit the potential

Table 8: Effect of Harmonious BN Update.

Methods	VOC (92)	City. ( $1/16$ )
Mean-Teacher	51.7	66.1
+HBN	61.5 +9.8	71.7 +5.6
CutMix-MT	52.2	68.3
+HBN	68.6 +16.4	73.2 +4.9
ReCo	64.8	71.4
+HBN	67.5 +2.7	75.1 +3.7
U2PL	68.0	70.3
+HBN	69.1 +1.1	72.4 +2.1
iMAS	68.8	74.3
+HBN	69.7 +0.9	75.1 +0.8
AugSeg	71.1	73.7
+HBN	74.1 +3.0	75.1 +1.4
SAMTH (no HBN)	62.8	69.4
SAMTH	70.7 +7.9	75.1 +5.7

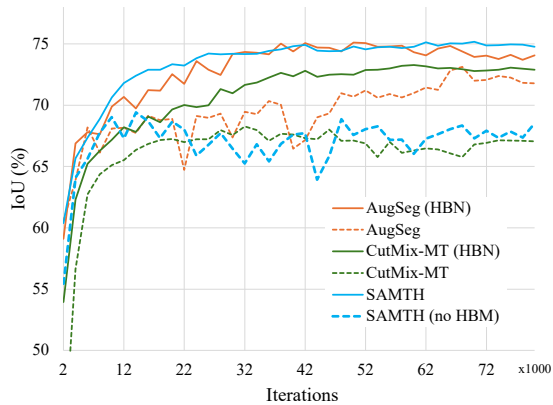


Figure 7: Training curves of AugSeg, CutMix-MT, and SAMTH. The bold lines are method trained with HBN update strategy, while the dotted lines are ones without.

of boundary cues, whereas our multi-faceted approach proves more effective in the SS-SS context.

### 4.3.5 Effect of Harmonious BN update strategy

To further examine the effect of our Harmonious Batch Normalization (HBN) update strategy, we compare different BN update approaches in Tab. 8. Methods like CutMix-MT, ReCo, and U2PL also update the teacher’s BN statistics via forward passes. However, unlike HBN (which processes the complete batch through the teacher specifically for BN updates, as described in Sec. 3.3), these methods often introduce discrepancies between the inputs used for the teacher’s BN statistics and the student’s training inputs. Other approaches, such as iMAS and AugSeg, update the teacher’s BN buffers via EMA based on the student’s statistics. As demonstrated in the table, incorporating our HBN strategy consistently yields significant improvements in segmentation performance across various base methods. For example, applying HBN to SAMTH results in a 5.7% absolute improvement in mean IoU on Cityscapes (from 69.4% to 75.1%). The training curves in Fig. 7 provide further evidence, indicating that HBN stabilizes the training process and accelerates convergence, thus highlighting its practical benefits.

Table 9: Computation Cost of methods. We report the average iteration time in seconds and the GPU memory requirements of a single GPU during **training**. We also report FLOPs, number of parameters, and FPS during **inference**.

Methods	IoU	Time	Memory	FLOPs	Params	FPS
UniMatch	75.3	1.21s	20.6G	191G	40.5M	23.4
SAMTH	75.1	0.92s	9.0G	191G	40.5M	23.4
+BoundMatch	76.4	1.59s	16.5G	192G	40.6M	19.0

Table 10: Evaluation of methods in a more real-world semi-supervised setting where we use the entire labeled Cityscapes dataset (2975 images) along with the *extra* 19997 unlabeled training data. We evaluate under the same setting for all methods and use ResNet-50 as the backbone.

Method	IoU	BIoU	BF1
Supervised Only	77.58	57.73	60.06
UniMatch	80.18	61.18	67.43
SAMTH	80.26	60.86	65.21
+BoundMatch	80.83	62.24	69.02

### 4.3.6 Computational Cost

Tab. 9 summarizes the computational cost of our approach in terms of inference time and memory consumption. Although SAMTH+BoundMatch incurs a higher computational overhead compared to the baseline UniMatch and SAMTH (with inference time increasing from 0.92 s to 1.59 s and memory usage from 9.0 G to 16.5 G), the performance gains in segmentation accuracy (with IoU increasing to 76.38%) justify the additional cost. The memory usage increases in the boundary detection head due to convolution of spatially large feature maps from the early stages of the backbone. This trade-off is especially acceptable in scenarios where segmentation precision is of paramount importance. Furthermore, the computational cost of SAMTH+BoundMatch is still comparable to that of UniMatch, while achieving better performance.

### 4.4 More Real-World SS-SS Setting

Inspired by the evaluation protocol in [47], we assess SS-SS in a realistic scenario: using all 2,975 Cityscapes training images as labeled data and the additional 19,997 “extra” images as truly unlabeled data. In this setting, the fully supervised baseline is already strong, making further gains challenging yet highly relevant for practical deployment. As shown in Tab. 10, SAMTH+BoundMatch achieves consistent improvements over both SAMTH and UniMatch, particularly in boundary-focused metrics (BIoU and BF1), demonstrating its effectiveness at leveraging large unlabeled pools in real-world applications.

### 4.5 Application to lightweight models

We further evaluate BoundMatch on lightweight segmentation architectures suitable for resource-constrained devices. Specifically, we apply our method to a MobileNet-V2 backbone [62] with DeepLabV3+ and to AFFormer-Tiny, a compact Transformer model [22]. For the latter, we compare against MobileSeed [12], a strong baseline for semi-supervised segmentation on AFFormer-Tiny.

Table 11: Lightweight segmentation architectures applied to the same setting as Tab. 10. Here “BoundMatch” refers to SAMTH+BoundMatch which is trained with the additional unlabeled *Extra* data. We use input size of  $768 \times 768$  and  $800 \times 800$  for MobileNet-V2 and AFFormer-Tiny, respectively.

Method		IoU	BloU	BF1	FLOPs	Params	FPS
DLV3+ MV2		73.4	53.9	56.5	89.7G	5.8M	36.0
	BoundMatch	78.2	59.0	64.3	93.7G	6.0M	31.8
AFFormer-Tiny		76.7	57.5	65.2	7.3G	2.1M	89.1
	Mobile-Seed	78.0	58.3	65.1	10.0G	2.4M	70.2
	BoundMatch	80.1	61.1	68.2	9.2G	2.2M	78.0

Results in Tab. 11 demonstrate that applying BoundMatch yields substantial gains in both overall accuracy and boundary quality metrics across both lightweight backbones. These accuracy improvements are achieved with only a minor increase in computational overhead (FLOPs and inference time), indicating a favorable trade-off between performance and efficiency compared to the original lightweight models.

Notably, when applied to AFFormer-Tiny, BoundMatch not only surpasses the segmentation quality of the specialized Mobile-Seed method but also achieves higher throughput (FPS) with slightly lower FLOPs. This highlights the efficiency benefits of our MTL architecture combined with SS-SS training on additional unlabeled data, even compared to methods specifically tailored for lightweight semi-supervised learning.

These findings confirm the BoundMatch framework’s flexibility and its effectiveness in enhancing performance even for models designed for real-time, low-compute deployment scenarios.

## 5 Conclusion and Future Work

In this paper, we introduced BoundMatch, a framework designed to mitigate the challenge of imprecise boundaries in semi-supervised semantic segmentation (SS-SS). BoundMatch integrates semantic boundary detection into the teacher-student consistency paradigm via our Boundary Consistency Regularized Multi-Task Learning (BCRM) approach. This core mechanism is enhanced by lightweight Boundary-Semantic Fusion (BSF) and Spatial Gradient Fusion (SGF) modules that improve boundary-segmentation synergy and pseudo-label quality, built upon SAMTH, our stable baseline incorporating Harmonious Batch Normalization (HBN).

Extensive experiments across diverse datasets, including Cityscapes, BDD100K, and SYNTHIA, demonstrate that BoundMatch achieves competitive segmentation accuracy while significantly improving boundary-specific evaluation metrics. Furthermore, its effectiveness was validated in scenarios involving large-scale unlabeled data and on lightweight architectures suitable for deployment. Overall, our work highlights the substantial benefits of explicit boundary modeling and consistency regularization within the SS-SS paradigm.

Future research directions include extending the principles of BoundMatch to related tasks such as 3D segmentation and depth estimation. We also plan to investigate potential refinements to the boundary prediction and fusion modules, as well as explore the integration of these techniques with modern visual

foundation models for advancing SS-SS capabilities. Our overarching goal remains to develop annotation-efficient learning methods that enable robust perception for real-world robotic and autonomous systems.

## References

- [1] Marius Cordts, Mohamed Omran, Sebastian Ramos, Timo Rehfeld, Markus Enzweiler, Rodrigo Benenson, Uwe Franke, Stefan Roth, and Bernt Schiele. The cityscapes dataset for semantic urban scene understanding. *2016 IEEE Conference on Computer Vision and Pattern Recognition (CVPR)*, pages 3213–3223, 2016.
- [2] Mohammed A. M. Elhassan, Changjun Zhou, Ali Khan, Amina Benabid, Abuzar B. M. Adam, Atif Mehmood, and Naftaly Muriuki Wambugu. Real-time semantic segmentation for autonomous driving: A review of cnns, transformers, and beyond. *J. King Saud Univ. Comput. Inf. Sci.*, 36:102226, 2024.
- [3] F. Xia, Amir Roshan Zamir, Zhi-Yang He, Alexander Sax, Jitendra Malik, and Silvio Savarese. Gibson env: Real-world perception for embodied agents. *2018 IEEE/CVF Conference on Computer Vision and Pattern Recognition (CVPR)*, pages 9068–9079, 2018.
- [4] Medhini Narasimhan, Erik Wijmans, Xinlei Chen, Trevor Darrell, Dhruv Batra, Devi Parikh, and Amanpreet Singh. Seeing the un-scene: Learning amodal semantic maps for room navigation. *ArXiv*, abs/2007.09841, 2020.
- [5] Huimin Huang, Lanfen Lin, Yue Zhang, Yingying Xu, Jing Zheng, Xiongwei Mao, Xiaohan Qian, Zhiyi Peng, Jianying Zhou, Yenwei Chen, and Ruofeng Tong. Graphbas3net: Boundary-aware semi-supervised segmentation network with bilateral graph convolution. *2021 IEEE/CVF International Conference on Computer Vision (ICCV)*, pages 7366–7375, 2021.
- [6] Rushi Jiao, Yichi Zhang, Leiting Ding, Rong Cai, and Jicong Zhang. Learning with limited annotations: A survey on deep semi-supervised learning for medical image segmentation. *Computers in biology and medicine*, 169:107840, 2022.
- [7] Liwei Huang, Bitao Jiang, Shouye Lv, Yanbo Liu, and Ying Fu. Deep-learning-based semantic segmentation of remote sensing images: A survey. *IEEE Journal of Selected Topics in Applied Earth Observations and Remote Sensing*, 17:8370–8396, 2024.
- [8] Geoff French, Samuli Laine, Timo Aila, Michal Mackiewicz, and Graham Finlayson. Semi-supervised semantic segmentation needs strong, varied perturbations. In *BMVC*, 2020.
- [9] Lihe Yang, Lei Qi, Litong Feng, Wayne Zhang, and Yinghuan Shi. Revisiting weak-to-strong consistency in semi-supervised semantic segmentation. *2023 IEEE/CVF Conference on Computer Vision and Pattern Recognition (CVPR)*, 2022.
- [10] Towaki Takikawa, David Acuna, V. Jampani, and Sanja Fidler. Gated-scnn: Gated shape cnns for semantic seg-

- mentation. *2019 IEEE/CVF International Conference on Computer Vision (ICCV)*, pages 5228–5237, 2019.
- [11] Haruya Ishikawa and Yoshimitsu Aoki. Boosting semantic segmentation by conditioning the backbone with semantic boundaries. *Sensors (Basel, Switzerland)*, 23, 2023.
- [12] Youqi Liao, Shuhao Kang, Jianping Li, Yang Liu, Yun Liu, Zhen Dong, Bisheng Yang, and Xieyuanli Chen. Mobileseed: Joint semantic segmentation and boundary detection for mobile robots. *IEEE Robotics and Automation Letters*, 2024.
- [13] Shuo Li, Yue He, Weiming Zhang, Wei Zhang, Xiao Tan, Junyu Han, Errui Ding, and Jingdong Wang. Cfcg: Semi-supervised semantic segmentation via cross-fusion and contour guidance supervision. *2023 IEEE/CVF International Conference on Computer Vision (ICCV)*, pages 16302–16312, 2023.
- [14] Ebenezer Tarubinga and Jenifer Kalafatovich Espinoza. Confidence-weighted boundary-aware learning for semi-supervised semantic segmentation. *ArXiv*, 2025.
- [15] Yitong Li, Changlun Zhang, and Hengyou Wang. Boundaries matters: A novel multi-branch semi-supervised semantic segmentation method. *IEEE Intelligent Systems*, 2024.
- [16] Jonathan Long, Evan Shelhamer, and Trevor Darrell. Fully convolutional networks for semantic segmentation. *2015 IEEE Conference on Computer Vision and Pattern Recognition (CVPR)*, pages 3431–3440, 2015.
- [17] Hengshuang Zhao, Jianping Shi, Xiaojuan Qi, Xiaogang Wang, and Jiaya Jia. Pyramid scene parsing network. *2017 IEEE Conference on Computer Vision and Pattern Recognition (CVPR)*, pages 6230–6239, 2017.
- [18] Zhen Zhu, Mengde Xu, Song Bai, Tengpeng Huang, and Xiang Bai. Asymmetric non-local neural networks for semantic segmentation. *2019 IEEE/CVF International Conference on Computer Vision (ICCV)*, pages 593–602, 2019.
- [19] Enze Xie, Wenhai Wang, Zhiding Yu, Anima Anandkumar, José Manuel Álvarez, and Ping Luo. Segformer: Simple and efficient design for semantic segmentation with transformers. In *Advances in Neural Information Processing Systems (NeurIPS)*, 2021.
- [20] Liang-Chieh Chen, Yukun Zhu, George Papandreou, Florian Schroff, and Hartwig Adam. Encoder-decoder with atrous separable convolution for semantic image segmentation. In *2018 IEEE/CVF European Conference on Computer Vision (ECCV)*, 2018.
- [21] Changqian Yu, Changxin Gao, Jingbo Wang, Gang Yu, Chunhua Shen, and Nong Sang. Bisenet v2: Bilateral network with guided aggregation for real-time semantic segmentation. *International Journal of Computer Vision*, 129:3051 – 3068, 2020.
- [22] B. Dong, Pichao Wang, and Fan Wang. Head-free lightweight semantic segmentation with linear transformer. *ArXiv*, abs/2301.04648, 2023.
- [23] Xiangtai Li, Xia Li, Li Zhang, Guangliang Cheng, Jianping Shi, Zhouchen Lin, Shaohua Tan, and Yunhai Tong. Improving semantic segmentation via decoupled body and edge supervision. *2020 IEEE/CVF European Conference on Computer Vision (ECCV)*, abs/2007.10035, 2020.
- [24] Saining Xie and Zhuowen Tu. Holistically-nested edge detection. *International Journal of Computer Vision (IJCV)*, 125:3–18, 2015.
- [25] Yun Liu, Ming-Ming Cheng, Xiaowei Hu, Kai Wang, and Xiang Bai. Richer convolutional features for edge detection. *2017 IEEE Conference on Computer Vision and Pattern Recognition (CVPR)*, pages 5872–5881, 2017.
- [26] Zhiding Yu, Chen Feng, Ming-Yu Liu, and Srikumar Ramalingam. Casenet: Deep category-aware semantic edge detection. *2017 IEEE Conference on Computer Vision and Pattern Recognition (CVPR)*, pages 1761–1770, 2017.
- [27] Mingmin Zhen, Jinglu Wang, Lei Zhou, Shiwei Li, Tianwei Shen, Jiayang Shang, Tian Fang, and Quan Long. Joint semantic segmentation and boundary detection using iterative pyramid contexts. *2020 IEEE/CVF Conference on Computer Vision and Pattern Recognition (CVPR)*, pages 13663–13672, 2020.
- [28] Zhiding Yu, Rui Huang, Wonmin Byeon, Sifei Liu, Guilin Liu, Thomas Breuel, Anima Anandkumar, and Jan Kautz. Coupled segmentation and edge learning via dynamic graph propagation. In *Advances in Neural Information Processing Systems (NeurIPS)*, 2021.
- [29] Mingyuan Fan, Shenqi Lai, Junshi Huang, Xiaoming Wei, Zhenhua Chai, Junfeng Luo, and Xiaolin Wei. Rethinking bisenet for real-time semantic segmentation. *2021 IEEE/CVF Conference on Computer Vision and Pattern Recognition (CVPR)*, pages 9711–9720, 2021.
- [30] Hanzhe Hu, Fangyun Wei, Han Hu, Qiwei Ye, Jinshi Cui, and Liwei Wang. Semi-supervised semantic segmentation via adaptive equalization learning. In *Neural Information Processing Systems*, 2021.
- [31] Donghyeon Kwon and Suha Kwak. Semi-supervised semantic segmentation with error localization network. *2022 IEEE/CVF Conference on Computer Vision and Pattern Recognition (CVPR)*, pages 9947–9957, 2022.
- [32] Zicheng Wang, Zhen Zhao, Luping Zhou, Dong Xu, Xiaoxia Xing, and Xiangyu Kong. Conflict-based cross-view consistency for semi-supervised semantic segmentation. *2023 IEEE/CVF Conference on Computer Vision and Pattern Recognition (CVPR)*, pages 19585–19595, 2023.
- [33] Bo Sun, Yuqi Yang, Le Zhang, Ming-Ming Cheng, and Qibin Hou. Corrmatch: Label propagation via correlation matching for semi-supervised semantic segmentation. *2024 IEEE/CVF Conference on Computer Vision and Pattern Recognition (CVPR)*, pages 3097–3107, 2023.
- [34] Huayu Mai, Rui Sun, Tianzhu Zhang, and Feng Wu. Rankmatch: Exploring the better consistency regularization for semi-supervised semantic segmentation. *2024 IEEE/CVF Conference on Computer Vision and Pattern Recognition (CVPR)*, pages 3391–3401, 2024.

- [35] Xiaoyang Wang, Huihui Bai, Limin Yu, Yao Zhao, and Jimin Xiao. Towards the uncharted: Density-descending feature perturbation for semi-supervised semantic segmentation. *2024 IEEE/CVF Conference on Computer Vision and Pattern Recognition (CVPR)*, pages 3303–3312, 2024.
- [36] Jianjian Yin, Yi Chen, Zhichao Zheng, Junsheng Zhou, and Yanhui Gu. Uncertainty-participation context consistency learning for semi-supervised semantic segmentation. *ArXiv*, abs/2412.17331, 2024.
- [37] Zhen Zhao, Lihe Yang, Sifan Long, Jimin Pi, Luping Zhou, and Jingdong Wang. Augmentation matters: A simple-yet-effective approach to semi-supervised semantic segmentation. *2023 IEEE/CVF Conference on Computer Vision and Pattern Recognition (CVPR)*, pages 11350–11359, 2022.
- [38] Zhen Zhao, Sifan Long, Jimin Pi, Jingdong Wang, and Luping Zhou. Instance-specific and model-adaptive supervision for semi-supervised semantic segmentation. *2023 IEEE/CVF Conference on Computer Vision and Pattern Recognition (CVPR)*, pages 23705–23714, 2022.
- [39] Jaemin Na, Jung-Woo Ha, HyungJin Chang, Dongyoon Han, and Wonjun Hwang. Switching temporary teachers for semi-supervised semantic segmentation. *ArXiv*, abs/2310.18640, 2023.
- [40] Shikun Liu, Shuaifeng Zhi, Edward Johns, and Andrew J. Davison. Bootstrapping semantic segmentation with regional contrast. *ArXiv*, abs/2104.04465, 2021.
- [41] Yuchao Wang, Haochen Wang, Yujun Shen, Jingjing Fei, Wei Li, Guoqiang Jin, Liwei Wu, Rui Zhao, and Xinyi Le. Semi-supervised semantic segmentation using unreliable pseudo-labels. *2022 IEEE/CVF Conference on Computer Vision and Pattern Recognition (CVPR)*, pages 4238–4247, 2022.
- [42] Wooseok Shin, Hyun Joon Park, Jin Sob Kim, and Sung Won Han. Revisiting and maximizing temporal knowledge in semi-supervised semantic segmentation. *ArXiv*, abs/2405.20610, 2024.
- [43] Haikuan Zhang, Haitao Li, Xiufeng Zhang, Guanyu Yang, Atao Li, Weisheng Du, Shanshan Xue, and Chi Liu. Noise-robust consistency regularization for semi-supervised semantic segmentation. *Neural networks : the official journal of the International Neural Network Society*, 184:107041, 2024.
- [44] Qiankun Ma, Ziyao Zhang, Pengchong Qiao, Yu Wang, Rongrong Ji, Chang Liu, and Jie Chen. Dual-level masked semantic inference for semi-supervised semantic segmentation. *IEEE Transactions on Multimedia*, 2025.
- [45] Haonan Wang, Qixiang Zhang, Yi Li, and Xiaomeng Li. Allspark: Reborn labeled features from unlabeled in transformer for semi-supervised semantic segmentation. *2024 IEEE/CVF Conference on Computer Vision and Pattern Recognition (CVPR)*, pages 3627–3636, 2024.
- [46] Lukas Hoyer, David Joseph Tan, Muhammad Ferjad Naeem, Luc van Gool, and Federico Tombari. Semivl: Semi-supervised semantic segmentation with vision-language guidance. In *European Conference on Computer Vision*, 2023.
- [47] Lihe Yang, Zhen Zhao, and Hengshuang Zhao. Unimatch v2: Pushing the limit of semi-supervised semantic segmentation. *TPAMI*, 2025.
- [48] Fisher Yu, Haofeng Chen, Xin Wang, Wenqi Xian, Yingying Chen, Fangchen Liu, Vashisht Madhavan, and Trevor Darrell. Bdd100k: A diverse driving dataset for heterogeneous multitask learning. *2020 IEEE/CVF Conference on Computer Vision and Pattern Recognition (CVPR)*, pages 2633–2642, 2018.
- [49] Germán Ros, Laura Sellart, Joanna Materzynska, David Vázquez, and Antonio M. López. The synthia dataset: A large collection of synthetic images for semantic segmentation of urban scenes. *2016 IEEE Conference on Computer Vision and Pattern Recognition (CVPR)*, pages 3234–3243, 2016.
- [50] M. Everingham, L. Van Gool, C. K. I. Williams, J. Winn, and A. Zisserman. The PASCAL Visual Object Classes Challenge 2012 (VOC2012) Results. <http://www.pascal-network.org/challenges/VOC/voc2012/workshop/index.html>, 2012.
- [51] Bolei Zhou, Hang Zhao, Xavier Puig, Sanja Fidler, Adela Barriuso, and Antonio Torralba. Scene parsing through ade20k dataset. *2017 IEEE Conference on Computer Vision and Pattern Recognition (CVPR)*, pages 5122–5130, 2017.
- [52] MMSegmentation Contributors. MMSegmentation: Openmmlab semantic segmentation toolbox and benchmark. <https://github.com/open-mmlab/mms Segmentation>, 2020.
- [53] Chen Liang, Wenguan Wang, Jiaxu Miao, and Yi Yang. Logic-induced diagnostic reasoning for semi-supervised semantic segmentation. *2023 IEEE/CVF International Conference on Computer Vision (ICCV)*, pages 16151–16162, 2023.
- [54] Changqi Wang, Haoyu Xie, Yuhui Yuan, Chong Fu, and Xiangyu Yue. Space engage: Collaborative space supervision for contrastive-based semi-supervised semantic segmentation. *2023 IEEE/CVF International Conference on Computer Vision (ICCV)*, pages 931–942, 2023.
- [55] Yijiang Li, Xinjiang Wang, Lihe Yang, Litong Feng, Wayne Zhang, and Ying Gao. Diverse cotraining makes strong semi-supervised segmentor. *2023 IEEE/CVF International Conference on Computer Vision (ICCV)*, pages 16009–16021, 2023.
- [56] Rui Sun, Huayu Mai, Tianzhu Zhang, and Feng Wu. Daw: Exploring the better weighting function for semi-supervised semantic segmentation. In *Neural Information Processing Systems*, 2023.
- [57] Jie Ma, Chuan Wang, Yang Liu, Liang Lin, and Guanbin Li. Enhanced soft label for semi-supervised semantic segmentation. *2023 IEEE/CVF International Conference on Computer Vision (ICCV)*, pages 1185–1195, 2023.

- 
- [58] Kebin Wu, Wenbin Li, and Xiaofei Xiao. Ipixmatch: Boost semi-supervised semantic segmentation with inter-pixel relation. *2024 International Joint Conference on Neural Networks (IJCNN)*, pages 1–7, 2024.
  - [59] Hao Li, Chenxin Tao, Xizhou Zhu, Xiaogang Wang, Gao Huang, and Jifeng Dai. Auto seg-loss: Searching metric surrogates for semantic segmentation. *ArXiv*, abs/2010.07930, 2020.
  - [60] Pushmeet Kohli, Lubor Ladicky, and Philip H. S. Torr. Robust higher order potentials for enforcing label consistency. *International Journal of Computer Vision*, 82:302–324, 2008.
  - [61] Gabriela Csurka, Diane Larlus, and Florent Perronnin. What is a good evaluation measure for semantic segmentation? In *British Machine Vision Conference*, 2013.
  - [62] Mark Sandler, Andrew G. Howard, Menglong Zhu, Andrey Zhmoginov, and Liang-Chieh Chen. Mobilenetv2: Inverted residuals and linear bottlenecks. *2018 IEEE/CVF Conference on Computer Vision and Pattern Recognition*, pages 4510–4520, 2018.